Journal of Materials Science & Technology 104 (2022) 236–243

Contents lists available at ScienceDirect

Journal of Materials Science & Technology

journal homepage: www.elsevier.com/locate/jmst

Research Article

Lattice distortion and magnetic property of high entropy alloys at low temperatures

Yuan-Yuan Tan[a,1], Zhong-Jun Chen[b,1], Ming-Yao Su[a,c], Gan Ding[a], Min-Qiang Jiang[a,c], Zhou-Can Xie[a,c], Yu Gong[b], Tao Wu[d], Zhong-Hua Wu[b], Hai-Ying Wang[a,c], Lan-Hong Dai[a,c,e,*]

[a] State Key Laboratory of Nonlinear Mechanics, Institute of Mechanics, Chinese Academy of Sciences, Beijing 100190, China
[b] Institute of High Energy Physics, Chinese Academy of Sciences & Graduate, University of Chinese Academy of Sciences, Beijing 100049, China
[c] School of Engineering Science, University of Chinese Academy of Sciences, Beijing 100049, China
[d] Zhejiang Institute of Mechanical & Electrical Engineering, Hangzhou 310053, China
[e] State Key Laboratory of Explosion Science and Technology, Beijing Institute of Technology, Beijing 100081, China

ARTICLE INFO

Article history:
Received 4 February 2021
Revised 6 July 2021
Accepted 7 July 2021
Available online 12 September 2021

Keywords:
High entropy alloy
Lattice distortion
Magnetic property
Low temperature
In situ SR-XRD

ABSTRACT

Deformation mechanisms and magnetic properties of medium and high entropy alloys (MEA/HEAs) closely relate to lattice distortion and are strongly temperature-dependent, in particular, at low temperature ranges. However, little attention has been paid to the evolution of lattice distortion with temperature decreasing and its effects on deformation behavior and magnetic state transition. In this work, we carry out *in situ* synchrotron radiation based X-ray powder diffraction (SR-XRD) experiments from 293 to 123 K aiming for determining lattice distortion evolutions of CrCoNi MEA, CrFeCoNi and CrMnFeCoNi HEAs. Magnetic measurements at corresponding low temperatures and cryogenic ranges are further conducted. The *in situ* SR-XRD results demonstrate a general reduction of lattice distortion magnitude with temperature decreasing, which shows a similar tendency with that of reported stacking fault energy (SFE) values. It is thus suggested that lattice distortion reduction possibly makes a critical contribution to deformation mechanism transition. The magnetic measurement results show a clear ferromagnetic transition of CrFeCoNi HEA when temperature is below 173 K. While, no obvious magnetic state transition is observed for CrCoNi MEA and CrMnFeCoNi HEA. The present findings on lattice distortion evolutions will pave the way for designing targeted HEAs with particular properties.

1. Introduction

Since the first inception in 2004 [1,2], medium and high entropy alloys (MEA and HEA) have been attracting increasing research enthusiasm due to their unprecedented properties [3–6]. Lattice distortion is one of the four core effects of HEAs [2,7]. It plays a vital role of importance on mechanical performance [8–10], solid solution strengthening [11,12], phase stability [13,14], magnetic property [15,16], and etc. Synchrotron radiation based X-ray diffraction (SR-XRD) is one of the powerful experiment techniques for investigating lattice distortions [17–19] besides X-ray absorption fine structure (XAFS) [20,21], HRTEM [10] and other methods. X-ray diffraction data collected at a synchrotron radiation source could provide detailed lattice structure evolutions from Bragg peaks, such as position shift, intensity variation and full width at half maximum (FWHM) [22]. Normally, three types of strains are conventionally defined and classified contributing to Bragg peak variations [23]. Type I strain is usually referred to macroscopic and near homogeneous one from applied bulk stresses, which would cause inter-planar spacing increasing or decreasing, presented as Bragg peak position shifting. Type II strain is generally inhomogeneous and acts at a shorter distance than Type I, it mainly causes variations of grain orientations. Type III strain corresponds to variations within a crystal arising from local perturbations such as defects, leading to broadening of Bragg peaks. Lattice distortions in HEAs would be significantly affected by the applied temperature loadings, since defect movements and atomic thermal oscillations would be dramatically altered. Thus, more de-

* Corresponding author.
E-mail address: lhdai@lnm.imech.ac.cn (L.-H. Dai).
[1] The two authors contributed equally to this paper.

https://doi.org/10.1016/j.jmst.2021.07.019
1005-0302/

tails of lattice distortion evolutions with temperature are needed to clarify its effects on temperature dependences of deformation mechanism transformation and magnetic state transition.

The extensively studied CrCoNi MEA [24–26], CrFeCoNi [27,28] and CrMnFeCoNi HEAs [29–31] have been reported breaking out the strength-ductility trade-off at low and cryogenic temperatures. The dominated deformation mechanism would change from dislocation planar-slip to a synergy of dislocation and stacking faults and/or deformation-induced twinning with temperature decreasing [32]. Normally, it is not difficult to understand the strength increase at lower temperatures due to the deactivation of dislocation activities [33]. Surprisingly, the ductility significantly increases simultaneously, which is attributed to the participation of twinning at earlier deformation stages. The activation of twinning has been captured in detail by high-resolution transmission electron microscope (HRTEM) [34]. It is known that twinning takes place more easily in alloys with lower stacking fault energy (SFE), which represents well the energy associated with interrupting normal stacking sequence of crystal planes [35]. Although the observation of twinning at low temperature is proposed due to the corresponding decrease of SFE [36], little attention has been paid to the nature of temperature-dependence of SFE in alloys [37–39]. Nevertheless, very few experiments [40] have been reported on lattice structure evolution and its correlation with SFE as a function of temperature decreasing.

The magnetism of HEAs is another noticeable feature closely related to their local lattice structures [15,16], and is highly temperature-dependent, in particular, at low temperatures [41]. However, the reported theoretical results on the magnetism transformations at low and/or cryogenic temperature ranges are not consistent well [42,43]. Since the HEAs consist of multiple main component elements, a chemically disordered and topologically distorted crystal lattice would be formed, which makes magnetism of HEAs rather complex. For instance, in CrMnFeCoNi HEA systems, the Fe, Co, and Ni are ferromagnetic while Cr and Mn are antiferromagnetic. Thus, some calculations predicted parallel alignment of Fe, Co and Ni, but antiparallel alignment of Cr and Mn [44]. However, another theoretical study presented different magnetic moments of the composition elements, particularly, for Ni [45]. Evidently, the addition of new element such as Al, Ga, and Sn would change the paramagnetic state of CrFeCoNi-*X* (where *X* stands for the newly added element) to ferromagnetic at room temperature [46]. The phase transformation is usually observed at the same time. Thus, it is difficult to clarify the magnetic transition to the change of alloying composition, or the change of phase structure. Therefore, further investigations of the magnetic state of the CrMnFeCoNi HEAs are urgent to clarify the above-discussed debate.

Admittedly, temperature plays an important role in lattice structures and eventually chemical and magnetic interactions [47], and detailed information on atomic-scale lattice structure evolution at low temperatures could admittedly provide critical clues on understanding lattice distortion effects on deformation mechanism [41,42] and magnetic state transition [48]. A profound understanding of lattice structure evolution as a function of temperature will surely pave the way for designing targeted HEAs with outstanding mechanical properties for special requirements. Hence, the objective of the present paper is to experimentally determine lattice distortion evolutions as a function of temperature decreasing and attempt to uncover the temperature dependence of magnetic property. Therefore, in this work, we conducted *in situ* SR-XRD experiments of CrCoNi MEA, CrFeCoNi and CrMnFeCoNi HEAs from room temperature to 123 K. The magnetic properties are further measured at corresponding and further cryogenic temperatures (5 K), attempting to decipher correlations between lattice distortion and its effects on deformation behavior and magnetic state.

2. Materials and methods

Equiatomic CrCoNi MEA, CrFeCoNi HEA and CrMnFeCoNi HEA with equiaxed grain of $\sim$ 20 μm were produced from the same bulk alloys reported in our previous work [20]. Briefly, the ingots were prepared by arc melting for five times and homogenized at 1473 K for 24 h, air cooling, cold rolling, and annealing (1073 K, 1 h) for lattice distortion investigations. The *in situ* low temperature SR-XRD measurements were carried out at 4B9A beamline in Beijing Synchrotron Radiation Facility (BSRF) with an incident X-ray wavelength of 1.5406 Å. During the data collection, the sample with a size of 7 mm $\times$ 7 mm $\times$ 1 mm was put in the vacuum chamber of a low temperature furnace (Anton Paar TTK 450), which was equipped on a 6 circle diffractometer. The temperature and temperature decreasing rate (10 K/min) was controlled by liquid N_2 flow. To ensure the stability of sample temperature during measurements, the designated temperature was kept for 30 min before XRD pattern collections. The individual XRD pattern was collected from a 2θ angle of 35° to 105° with a scanning step of 0.02°. The collection time for a single XRD pattern is around 2 h. 12 XRD patterns were collected at 293, 223, 173 and 123 K for CrCoNi MEA, CrFeCoNi HEA and CrMnFeCoNi HEA, respectively. All the XRD data have been normalized before refinement analysis to exclude the effect of incident beam decay over a long time. Standard Si powders were measured at the same time to determine instrument broadening.

Magnetic measurements were carried out by using a vibrating sample magnetometer (VSM) equipped on the Dynacool PPMS system from American Quantum Design with a temperature stability better than ±0.2% and a magnetism resolution higher than 0.2 mT. Magnetization hysteresis loops (*M-H* curves) were measured at 293, 223, 173, 150, 123, 77, 25 and 5 K in a magnetic field range from −5 to 5 T. The temperature dependence of the magnetic moment (*M-T* curve) was investigated in a temperature range from 300 to 4 K under a magnetic field of 200 Oe.

3. Results and discussion

3.1. Lattice structure variations

Fig. 1 shows XRD patterns of CrCoNi MEA (Fig. 1(a)), CrFeCoNi HEA (Fig. 1(b)) and CrMnFeCoNi HEA (Fig. 1(c)) collected at 293, 223, 173 and 123 K. All three alloys are kept face-centered cubic (FCC) structures at all the measured temperatures, and no distinct phase transformation is observed. The background intensity for each data changes little with temperature. However, the background intensities for CrCoNi MEA and CrFeCoNi HEA are relatively higher than those for CrMnFeCoNi HEA. This is possibly due to the fluorescence effect of higher Cr content in CrCoNi HEA, since the wavelength of Cr is longer than others [49]. The strongest diffraction peak in CrCoNi MEA is (220), while (111) peaks are the strongest ones in CrFeCoNi and CrMnFeCoNi HEAs. Since we focus on the evolutions of lattice distortion, the slightly preferred orientation in CrCoNi MEA is not an important factor as that in the studies focusing on the effects of alloy composition on local lattice distortion. Obvious peak position shiftings to higher two theta angle are observed for CrCoNi MEA, CrFeCoNi HEA and CrMnFeCoNi HEA with temperature decreasing, particularly, the positions of higher angle diffraction peaks, indicating continuous lattice contractions.

Individual peak position shifts of collected XRD patterns are quantified and shown in Fig. 2. Generally, the peak positions of (111), (200), (220) and (311) in CrCoNi MEA in Fig. 2(a) are higher than the corresponding ones in CrFeCoNi HEA in Fig. 2(b) and CrMnFeCoNi HEA in Fig. 2(c). This indicates a smaller lattice parameter of CrCoNi MEA than those of CrFeCoNi and CrMnFeCoNi HEAs. The

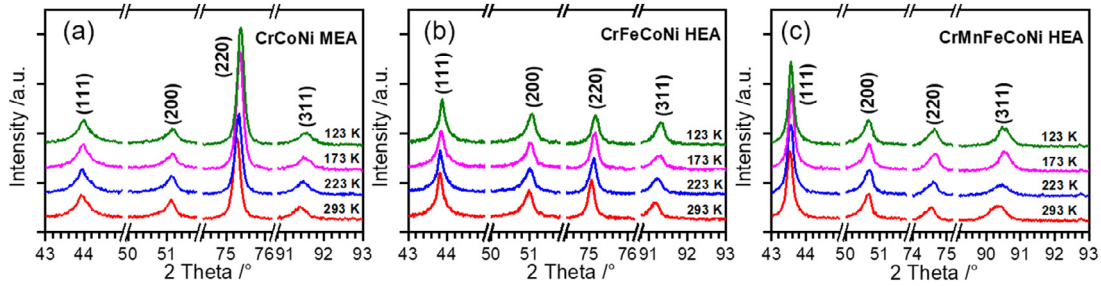

Fig. 1. XRD patterns of (a) CrCoNi MEA, (b) CrFeCoNi HEA and (c) CrMnFeCoNi HEA at 293, 223, 173, and 123 K collected at 4B9A beamline in BSRF.

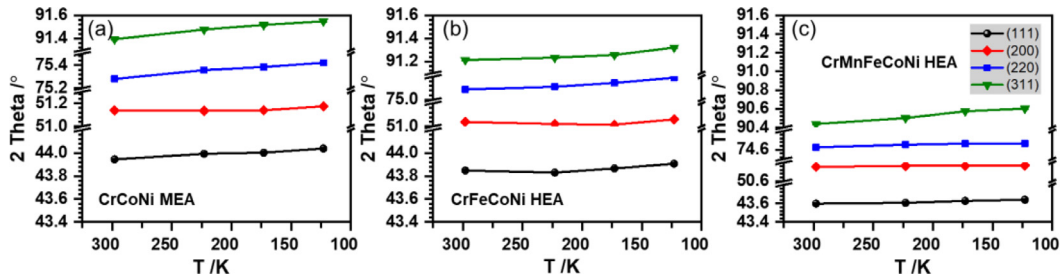

Fig. 2. (111), (200), (220) and (311) Bragg peak position shifts of (a) CrCoNi MEA, (b) CrFeCoNi HEA, (c) CrMnFeCoNi HEA. The error bars are very small and enclosed in the scattering symbols.

peak positions in each alloy increase almost linearly with decreasing temperature in the whole studied temperature range, implying a continuous contraction of lattice parameters of the three alloys. However, the peak position increases in CrCoNi MEA and CrFeCoNi HEA are slow from 293 to 173 K, but the accelerated increase of peak position shifts is observed from 173 to 123 K. While, the peak position increases of (111) and (200) in CrMnFeCoNi HEA are relatively higher in the studied temperature range. On the contrary, the peak position increasing behaviors of (220) and (311) planes in Fig. 2(a) and (c) are similar for CrCoNi MEA and CrMnFeCoNi HEA. Simultaneously, a little speeding up increase of peak positions for CrFeCoNi HEA is observed. Since the absolute values of corresponding *d* spacing of (111) and (200) peaks are larger than those for (220) and (311) peaks, the peak position shifts of (220) and (311) peaks are more sensitive and thus present larger magnitude of increase. However, differences are still observed among the magnitude evolutions of each peak position shifts at different temperature ranges, which is indicative of lattice distortion variations during temperature decreasing. Diffraction peak shape evolutions, such as peak intensity and full width at half maximum (FWHM), are also observed as a function of temperature, particularly at 173 K, which implies complex lattice distortions caused by temperature decreasing. The variations of peak shape would be discussed in detail after Rietveld refinement of the XRD patterns.

Rietveld refinements of all the collected XRD patterns are performed by Highscore Plus software [50] to obtain detailed lattice structure evolution information with temperature decreasing. The refinement details are shown in Figs. S1-S3 in Supplementary Materials. The peak profile is modeled by a Pseudo-Voigt function corrected for asymmetry owing to axial divergence. The FWHM is calibrated using a standard Si powder sample measured at the same vacuum conditions without temperature loadings. The refinement results are shown in Fig. 3. Generally, at a given temperature, the lattice parameter increases from CrCoNi MEA to CrFeCoNi HEA, and becomes more pronounced for CrMnFeCoNi HEA. Evidently, solid-solutioning more elements, such as Fe and Mn, to CrCoNi MEA would cause expansion of the lattice in the CrMnFeCoNi HEA system, and more detailed discussions about alloying composition effects on local lattice distortion are presented in our previous report [20]. Fig. 3(a) presents a linear lattice parameter decreasing of CrCoNi MEA, CrFeCoNi and CrMnFeCoNi HEAs from 293 to 123 K, indicating a generally linear lattice contraction, which agrees well with decreasing tendency of SFE [36,51]. The expansion coefficients for CrCoNi MEA, CrFeCoNi and CrMnFeCoNi HEAs are obtained from linear fittings and displayed as $(3.68\pm1.1)\times10^{-5}$, $(4.69\pm1.7)\times10^{-5}$, and $(8.96\pm1.5)\times10^{-5}$ /K, respectively. The values are in the same order but more than three times larger than those measured by Laplanche et al. [52,53] in similar and higher temperature ranges. Evidently, CrMnFeCoNi HEA has the largest lattice parameter and it decreases faster than those of CrFeCoNi HEA and CrCoNi MEA. Supposing that the lattice contraction rates for the alloys are the same in the low and cryogenic temperature ranges, the lattice parameters of CrCoNi MEA, CrFeCoNi and CrMnFeCoNi HEAs at 0 K are calculated to be (3.5605±0.0004) Å, (3.5676±0.0001) Å, and (3.5540±0.0002) Å, respectively. These values are similar to those reported in the theoretical calculations [21,54]. Hence, we propose that differences in lattice contraction rate for the alloys are possibly the main contributor to the contrary between measured lattice parameters at room temperature and lattice parameters calculated at 0 K.

To further explore the evolutions of local lattice distortion, the isotropic thermal motion factor (U_{iso}) in Eq. (1) is refined and displayed in Fig. 3(b).

$$8\pi^2 U_{iso} = \frac{6h^2}{mk\Theta_D^2}\left[\frac{\phi(x)}{x}+\frac{1}{4}\right]+d^2 \tag{1}$$

with $x=\frac{\Theta_D}{T}x=\frac{\Theta_D}{T}$, and $\phi(x)=\frac{1}{x}\int_0^x \frac{\xi}{e^{\xi}-1}\mathrm{d}\xi\,\phi(x)=\frac{1}{x}\int_0^x \frac{\xi}{e^{\xi}-1}\mathrm{d}\xi$

where h is Planck's constant, T the measurement temperature, m the atomic mass, k the Boltzmann constant, Θ_D the Debye temperature, and d^2 stands for static disorder in lattice. Eq. (1) has been used to describe contributions of static displacement and thermal dynamic displacement of lattice distortions [55,56] following Debye model. The first term is attributed to thermal dynamic displacement and the second term is considered to arise from static displacement. Therefore, U_{iso} in Fig. 3(b) describes a summation of static and dynamic displacements from the Rietveld refinement. At

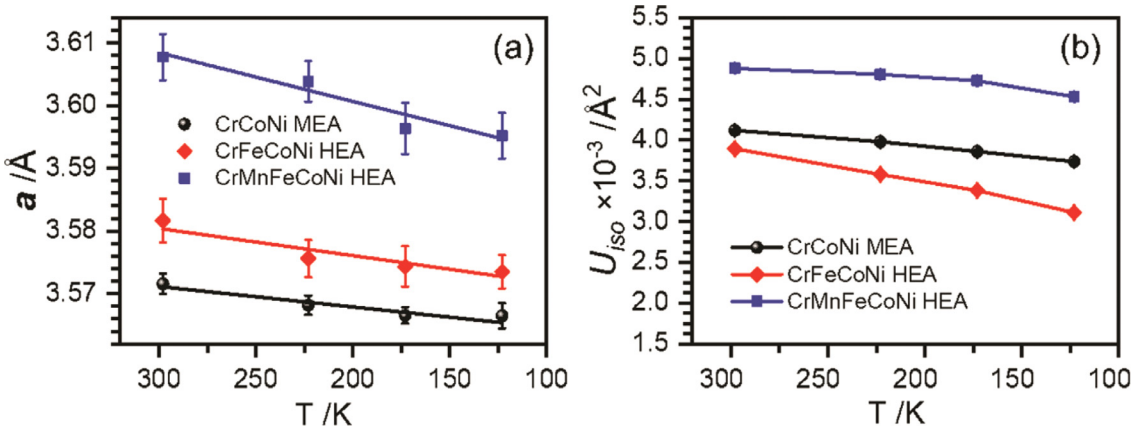

Fig. 3. (a) Lattice parameter and (b) U_{iso} evolutions of CrCoNi MEA, CrFeCoNi HEA and CrMnFeCoNi HEA along with temperature decreasing. The values are obtained from the Rietveld refinements of individual XRD patterns.

temperatures above 173 K, U_{iso} decreases approximately in linear for all three alloys, suggesting a smooth lattice distortion evolution in this temperature range. The variations of U_{iso} are well consistent with that of peak position shifts as shown in Fig. 2. These observations further verified that slightly preferred orientation in CrCoNi MEA has little effect on evolutions of lattice distortion with temperature. However, a change of slope in the temperature dependence of U_{iso} is observed when the temperature reaching 123 K for CrMnFeCoNi HEA, and it becomes more pronounced for CrFeCoNi HEA, indicating that a precursor lattice instability change may occur at 173 K. In general, the U_{iso} value in Fig. 3(b) for CrMnFeCoNi HEA is higher than those of CrCoNi MEA and CrFeCoNi HEA, suggesting the higher magnitude of lattice distortion for CrMnFeCoNi HEA at a certain temperature, which could arise from the increased number of composition alloying elements, specifically, chemical complexity. Similarly, the U_{iso} of CrCoNi MEA is slightly higher than that of CrFeCoNi HEA at 293 K, but the differences kept increasing with lowering temperature. A relatively faster decreasing rate is observed for CrFeCoNi HEA, and possibly, some local ordered structure is formed. Presumably, introducing Fe to CrCoNi MEA could effectively drive lattice distortion due to local microstrain field modification [56]. However, the addition of Mn to CrFeCoNi HEA has balanced the effect of Fe addition, since CrMnFeCoNi HEA shows a similar decreasing rate of U_{iso} with CrCoNi MEA. The decreasing of U_{iso} verifies reductions of lattice distortion in the alloys from both static and dynamic displacements. Unfortunately, it is difficult to distinguish distortions caused by static displacement from that by thermal dynamic displacement. The variations of U_{iso} also indicate that the average lattice distortions differ significantly from the local lattice distortions determined by X-ray absorption fine structure spectrum (XAFS) [20]. It also noted that the variations of U_{iso} with temperature are different dramatically with that evolves with chemical composition [57]. The differences of the U_{iso} variations indicate differences of local lattice distortions among CrCoNi MEA, CrFeCoNi and CrMnFeCoNi HEAs at low temperatures.

3.2. Local lattice distortion evolutions

To further investigate local distortions of each diffraction plane, evolutions of Bragg peak shape including both peak intensity and FWHM were analyzed in detail by line profile fittings. As mentioned above, no mechanical loadings were applied in this study. Thus, the evolutions of peak intensity and FWHM are attributed solely to temperature. The variations of peak intensity and FWHM were calculated using XRD patterns collected at 293 K as references for each sample. The evolutions for (111), (200), (220) and (311) planes of CrCoNi MEA, CrFeCoNi HEA and CrMnFeCoNi HEA are displayed in Fig. 4. From 293 to 223 K, the variations of peak intensity and FWHM are not violently, particularly for CrMnFeCoNi HEA. The increase of peak intensity is always simultaneously accompanied with FWHM decreasing, attributing to the decrease of local lattice distortions, and this variation is in good agreement with the Debye model. The results indicate that the reductions of local lattice distortion in this temperature range are not significant for CrMnFeCoNi HEA but more pronounced for CrCoNi MEA and CrFeCoNi HEA.

From 223 to 173 K, violent variations were observed for all three alloys. For CrCoNi MEA, the intensity of (220) peak increases sharply, and a slight increase is observed for (111) peak. While both peak intensity and FWHM reductions are observed for (200) and (311) peaks. This suggests that the reduction of lattice distortion in CrCoNi MEA from 223 to 173 K is mainly contributed by (220) planes, possibly due to its preferred orientation. However, the local lattice distortion changes little as the temperature further decreases from 173 to 123 K. For CrFeCoNi HEA, splitting variations of peak intensity and FWHM are observed. In general, (111) peak intensity and FWHM kept the same variation tendency with that of the former temperature range, suggesting a continuous increase of its local disorder. Similar variation is observed for (311) peak but with lower amplitude. The changing tendencies of (200) and (220) are similar for peak intensity increasing and FWHM decreasing, suggesting a slight reduction of local distortions. Surprisingly, as the temperature decreases further from 173 to 123 K, peak intensities of (311), (200) and (111) increase noticeably with simultaneous decreasing of FWHM for (311), (200) and (111), but the peak shape variation of (220) shows an inverse tendency. Plausibly, the local lattice structure orders of CrFeCoNi HEA change dramatically in the temperature range of 223 to 123 K, some local ordered structures might be formed [56]. For CrMnFeCoNi HEA, the variations are much more regular from 223 to 173 K, and peak intensity increases simultaneously with FWHM decreasing for all the peaks but with different fluctuations. While the changes are very small when further decreasing the temperature from 173 to 123 K, presenting a very similar tendency with that of CrCoNi MEA. Apparently, the lattice distortion evolutions of CrCoNi MEA and CrMnFeCoNi HEA act similar with each other: slight changes in relatively higher temperature range, and pronounced variations in the moderate range, while faint changes are observed when further decreasing to cryogenic range. But for CrFeCoNi HEA, the more violent variations are observed from 173 K to possibly much lower and cryogenic temperatures. The lattice distortions in CrFeCoNi HEA are seemed

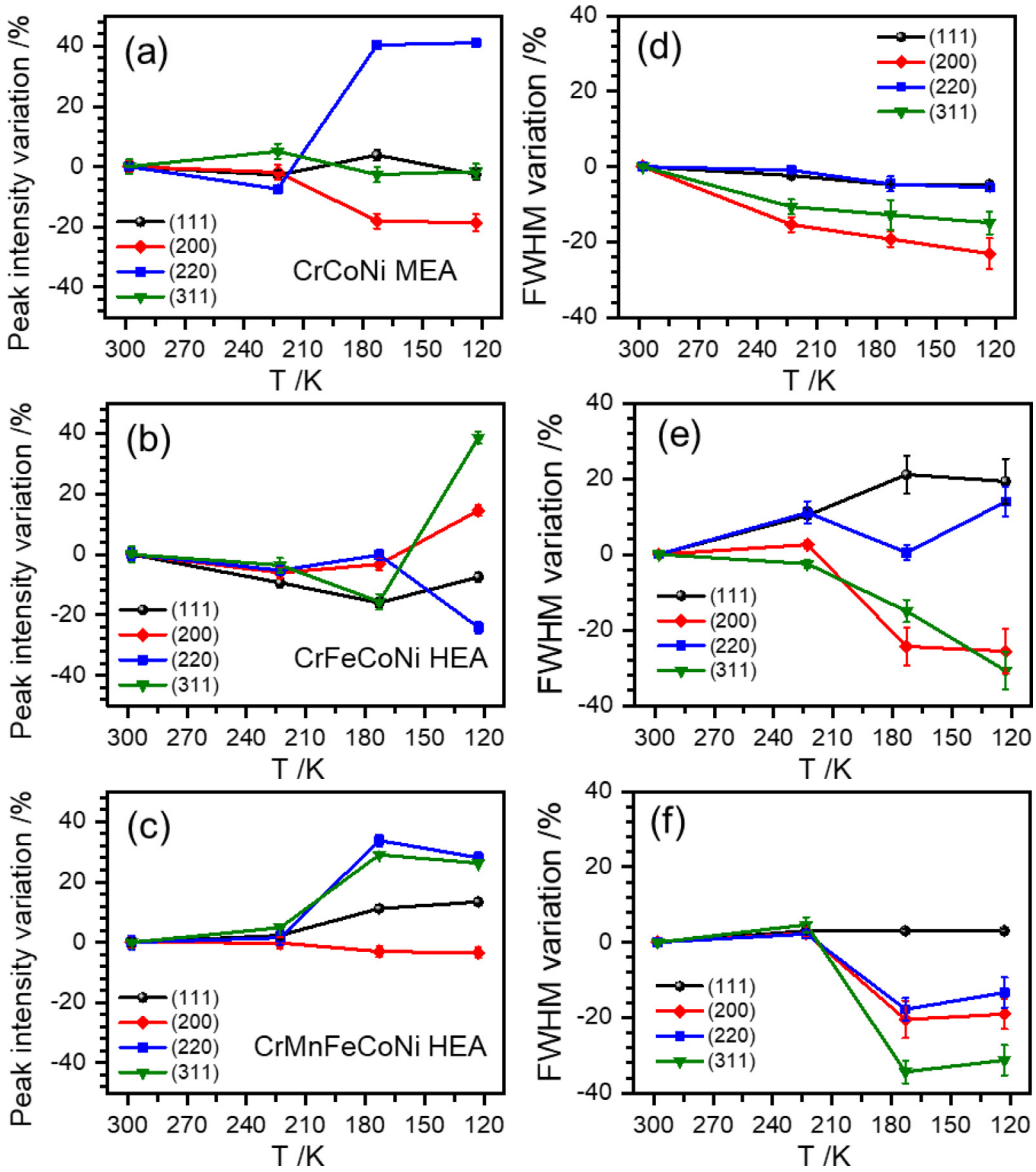

Fig. 4. (a-c) Peak intensity and (d-f) FWHM value evolutions for (111), (200), (220) and (311) planes of (a) CrCoNi MEA, (b) CrFeCoNi HEA and (c) CrMnFeCoNi HEA with decreasing temperature.

to be more complicated than those in CrCoNi MEA and CrMnFeCoNi HEA. The differences among lattice distortion evolutions of the three alloys might come from alloying composition and/or local magnetic property, since the pure composite metals are of different magnetic properties. The results demonstrate that when the temperature is applied to HEAs, lattice parameters and thermal oscillation will inevitably be forced to change. Thus, the applied temperature could be counted as Type I and Type III strains. The effects of lowering the temperature on lattice distortions in CrMnFeCoNi HEAs system are briefly described in Schematic 1.

3.3. Magnetic property at low and cryogenic temperatures

The magnetism of HEAs is another feature that is quite sensitive to their local lattice structure variations [15,16], particularly, the magnetic state at low temperatures is highly temperature-dependent [41]. As discussed in Section 3.2, the variations of lattice distortions in CrFeCoNi HEA are different from those of CrCoNi MEA and CrMnFeCoNi HEAs, suggesting a possibility of the formation of some local ordered structure that might alter the magnetic property of CrFeCoNi HEA at very low temperatures. On the other hand, the XRD patterns in Fig. 1 demonstrate that there are no phase structure transitions during the process of temperature decreasing, which will exclude the effect of phase change on the magnetic property of HEAs, and thus making the discussion on magnetic property simpler. Therefore, we measured not only magnetizations of CrCoNi MEA, CrFeCoNi and CrMnFeCoNi HEAs at 293, 223, 173, 150, 123 K, and further tested their magnetic properties at 77, 25 and 5 K to investigate correlations between lattice distortion evolutions and magnetic property of the three studied alloys.

The results shown in Fig. 5 demonstrate tremendous differences in the magnetization of CrFeCoNi HEA from those of CrCoNi MEA and CrMnFeCoNi HEA. In general, CrCoNi MEA, CrFeCoNi and CrMnFeCoNi HEAs are paramagnetic at ambient conditions in Fig. 5(b-d). However, as temperature further decreasing down to 5 K, an obvious magnetic state transition of CrFeCoNi HEA from paramagnetic to ferromagnetic state is observed in Fig. 5(a) and (c). By contrast, both CrCoNi MEA and CrMnFeCoNi HEA still keep in a paramagnetic state with slight magnetization increments in Fig. 5(b) and (d). The magnetization behavior of CrMnFeCoNi HEA is dif-

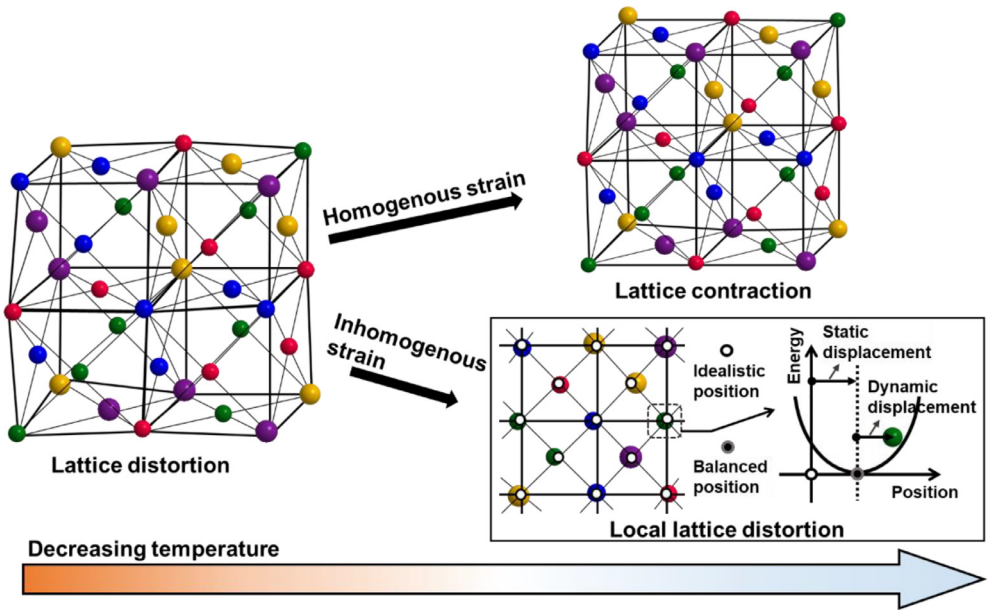

Schematic 1. Schematic of lowering temperature effects on lattice distortion evolutions in CrMnFeCoNi HEAs system.

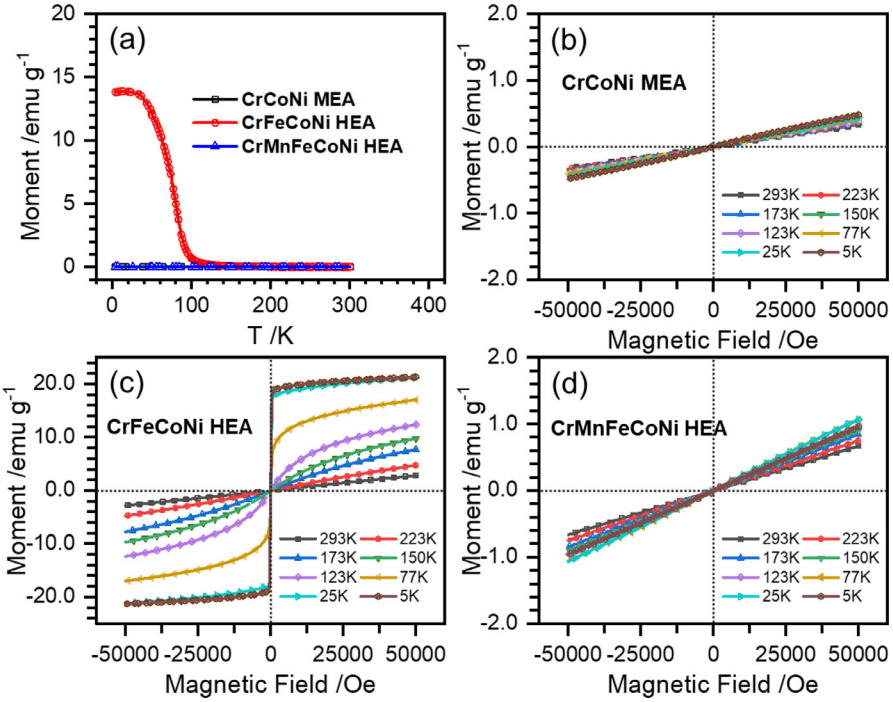

Fig. 5. Magnetic properties of CrCoNi MEA, CrFeCoNi and CrMnFeCoNi HEAs. (a) *M-T* curves collected at a temperature range from 300 to 4 K, (b-d) *M-H* curves measured at low and cryogenic temperatures.

ferent from that reported in the work of O. Schneeweiss et al. [43] and nanocrystalline CrMnFeCoNi HEA after special heat treatment [15]. Possibly, the differences come from heat treatment processes during the synthesis of the alloy. Upon lowering the temperature further, the magnetization of CrFeCoNi HEA grows gradually, the shape of *M-H* curves evolves from inclined saturation line toward a rectangular step around $H = 0$ at 25 and 5 K. The *M-H* curves from 150 to 5 K indicate soft magnetic characteristics of CrFeCoNi HEA starting at least from 25 K. As indicated in Fig. 5(a), the magnetic transition of CrFeCoNi HEA from paramagnetic to ferromagnetic is around 34 K, and stays approximately constant upon further cooling in Fig. 5(c). Evidently, the magnetization of CrFeCoNi HEA is dramatically different from that of CrCoNi MEA and CrMnFeCoNi HEA. Furthermore, this difference becomes obvious at 173 K, from which the lattice distortion evolutions of CrFeCoNi HEA become violent and apart from those of CrCoNi MEA and CrMnFeCoNi HEA. Thus, we infer that the sharp change of lattice distortions in CrFeCoNi HEA at this temperature range is mainly caused by the formation of some local magnetic orders. Surprisingly, we found that the formation of this kind of ordered magnetic structure speeds up in the cryogenic range from 123 to 25 K. Unfortunately, such lattice distortion information has not been collected in this work due to the limitation of experimental conditions. However, the ordered magnetic structure might approach saturation from 25 to 5 K. The magnetic state transition of CrFeCoNi HEA demonstrates that lattice distortion plays a role of crit-

ical importance on the magnetic property of CrFeCoNi HEA. Nevertheless, the magnetic evolutions of CrFeCoNi HEA from paramagnetic to soft ferromagnetic revealed CrFeCoNi HEA as a promising material for the application in magnetic sensing devices at low temperatures.

3.4. Discussions on lattice distortion, magnetic property and deformation behavior

Our results show clearly that lattice structures and magnetic properties of CrCoNi MEA, CrFeCoNi and CrMnFeCoNi HEAs go through dramatic changes as the temperature decreases from 293 to 123 and further 5 K. The lattice parameters decrease 1.425%, 2.278% and 3.476% for CrCoNi MEA, CrFeCoNi and CrMnFeCoNi HEAs, respectively. And CrFeCoNi HEA turns from paramagnetic into ferromagnetic state from room temperature to 5 K. It is reported that element composition and crystal structure have significant effects on magnetic properties of alloys [46,58]. In particular, for CrFeCoNi HEA, the substitution of Cr to Al or Ga will transform its paramagnetic state to ferromagnetic due to crystal lattice structure and/or phase changes [46,59]. However, the chemical composition and phase changes could be excluded in our study during the temperature cooling down process. No phase changes are observed for all the three alloys at least at 123 K, at which CrFeCoNi HEA has already changed into ferromagnetic state. The calculations results [59,60] suggest that the magnetic property of alloys has strong correlations with the magnetic exchange interactions among chemical compositions. The interactions depend mainly on the nearest-neighbor atom distances. For the CrFeCoNiAl HEA [59], its saturated ferromagnetic magnetization will be enhanced from FCC structure to body-centered cubic (BCC) structure with different Al contents. In this case, the ferromagnetic interactions among Fe-Fe, Fe-Co, and Co-Co atom pairs in BCC structure are supposed to be much stronger than those in the FCC structure. Possibly, the increase of magnetic property $CrFeCoNiAl_x$ HEA is caused by the elongation of nearest neighbor atom pair distances from $\frac{\sqrt{2}}{2}a$ in FCC to $\frac{\sqrt{3}}{2}a$ BCC (where a stands for the lattice parameter). However, in our case, the nearest neighbor atom pair distances in CrFeCoNi HEA during lowering temperature should be decreased due to lattice contraction. Thus, the magnetic state transition mechanism in our case might be different from the phase change. Nevertheless, these features demonstrate that lattice distortion has a strong impact on the magnetic property of CrFeCoNi HEA. On the contrary, the lattice distortion evolution works very little on the magnetic properties of CrCoNi MEA and CrMnFeCoNi HEA. Possibly, the giant magnetic difference of CrMnFeCoNi HEA from CrFeCoNi HEA might mainly arise from the addition of Mn [61,62], since spin state transition is observed in non-equiatomic CrMnFeCoNi alloy [41] and local magnetic moments of each alloy species have been reported to exhibit particular temperature and chemical dependency [16,47,63].

Based on the aforementioned discussions, it is clear that the effects of lowering temperature on lattice distortions are in good agreement with those on SFEs [35,64]. Since the theoretical calculations [65] demonstrate that the SFE of CrMnFeCoNi HEAs system will decrease with decreasing lattice distortion. Correspondingly, our results demonstrate that lattice distortions in CrMnFeCoNi HEAs system decreased with temperature cooling down, showing the same temperature dependence with that of SFE [36]. Furthermore, the lattice distortion of CrCoNi MEA is smaller than that of CrMnFeCoNi HEA at the studied temperature range, which on the other hand corresponds well with the lower SFE of CrCoNi MEA than that of CrMnFeCoNi HEA [66], explaining well on the mechanical performance of CrCoNi MEA superior to that of CrMnFeCoNi HEA due to earlier observation of twinning. Finally, the local lattice distortion reductions of CrMnFeCoNi HEA systems corresponding to each plane vary tremendously particularly below 223 K, which reminds us to consider the large variations on obtained values of SFE highly depending on local atomic structure. Thus, it is plausible to infer that variations of local lattice distortion in CrMnFeCoNi HEAs system cause significant differences in SFE values as demonstrated from computer-based calculations [65,67]. Therefore, we consider the general decrease of lattice distortion in CrMnFeCoNi HEAs system as a contributor to the decrease of SFE, while the variations of local lattice distortion might produce large differences on obtained SFE values.

But the magnetic property of HEAs might have little effect on their deformation behaviors. Although pronounced differences in magnetization were observed for CrFeCoNi HEA with those of CrCoNi MEA and CrMnFeCoNi HEA, similar deformation behaviors referred to the observation of serration in stress-strain curve were observed for both CrFeCoNi HEA [68] and CrMnFeCoNi HEA at 4.2 K [30]. Evidently, the three alloys exhibit similar deformation mechanisms at cryogenic temperatures, but their magnetic properties differ tremendously at corresponding temperatures. Hence, it is difficult to correlate the magnetic properties of CrMnFeCoNi HEAs with their deformation mechanism.

4. Conclusions

In summary, we carried out *in situ* SR-XRD experiments and magnetic measurements to investigate lattice distortion and magnetic property evolutions as a function of temperature from 293 to 123 K and to 5 K, respectively. The *in situ* SR-XRD results demonstrate that lowering temperature has significant effects on lattice structures of CrCoNi MEA, CrFeCoNi and CrMnFeCoNi HEAs. A linear lattice contraction and a general reduction of local lattice distortions for all three alloys were observed during decreasing temperature. The general reductions of lattice distortion in the CrMnFeCoNi HEAs system are in well agreement with the decreasing of reported SFE values as a function of temperature. However, the difference of lattice distortion evolution in CrFeCoNi HEA from that in CrCoNi MEA and CrMnFeCoNi HEA is detected from 173 K. Interestingly, the magnetic measurement results demonstrate a ferromagnetic transition for CrFeCoNi HEA starting at 173 K but not for CrCoNi MEA and CrMnFeCoNi HEA. Thus, some local ordered magnetic structure is supposed to be formed in CrFeCoNi HEA as the transition of ferromagnetic state. However, the three alloys show similar deformation behavior at cryogenic temperatures. Thus, we argue that magnetic property plays a minor role in the deformation behaviors of CrCoNi MEA, CrFeCoNi and CrMnFeCoNi HEAs. Nevertheless, it is striking to find that CrFeCoNi HEA is a promising candidate for soft magnetic materials at cryogenic temperatures.

Acknowledgements

This work is financially supported by the National Key Research and Development Program of China (No. 2017YFB0702003), the National Science Foundation of China (Nos. 12002341, 11790292 and 11672316), the NSFC Basic Science Center Program for “Multiscale Problems in Nonlinear Mechanics” (No. 11988102), the Strategic Priority Research Program (Nos. XDB22040302 and XDB22040303), the Key Research Program of Frontier Sciences (No. QYZDJSSW-JSC011), the Science Challenge Project (No. TZ2016001), the Zhejiang Provincial Natural Science Foundation (No. LGG21E010005).

Supplementary materials

Supplementary material associated with this article can be found, in the online version, at doi:10.1016/j.jmst.2021.07.019.

References

[1] B. Cantor, I.T.H. Chang, P. Knight, A.J.B. Vincent, Mater. Sci. Eng. A 375–377 (2004) 213–218.
[2] J.W. Yeh, S.K. Chen, S.J. Lin, J.Y. Gan, T.S. Chin, T.T. Shun, C.H. Tsau, S.Y. Chang, Adv. Eng. Mater. 6 (2004) 299–303.
[3] Z. Fu, L. Jiang, J.L. Wardini, B.E. MacDonald, H. Wen, W. Xiong, D. Zhang, Y. Zhou, T.J. Rupert, W. Chen, E.J. Lavernia, Sci. Adv. 4 (2018) 1–9.
[4] J.P. Liu, J.X. Chen, T.W. Liu, C. Li, Y. Chen, L.H. Dai, Scr. Mater. 181 (2020) 19–24.
[5] X.F. Liu, Z.L. Tian, X.F. Zhang, H.H. Chen, T.W. Liu, Y. Chen, Y.J. Wang, L.H. Dai, Acta Mater. 186 (2020) 257–266.
[6] Y.Z. Tian, S.J. Sun, H.R. Lin, Z.F. Zhang, J. Mater. Sci. Technol. 35 (2019) 334–340.
[7] Y. Zhang, T.T. Zuo, Z. Tang, M.C. Gao, K.A. Dahmen, P.K. Liaw, Z.P. Lu, Prog. Mater. Sci. 61 (2014) 1–93.
[8] L. Li, Q. Fang, J. Li, B. Liu, Y. Liu, P.K. Liaw, Mater. Sci. Eng. A 784 (2020) 139323.
[9] S.S. Sohn, A. Kwiatkowski da Silva, Y. Ikeda, F. Körmann, W. Lu, W.S. Choi, B. Gault, D. Ponge, J. Neugebauer, D. Raabe, Adv. Mater. 31 (2019) 1807142.
[10] C. Lee, Y. Chou, G. Kim, M.C. Gao, K. An, J. Brechtl, C. Zhang, W. Chen, J.D. Poplawsky, G. Song, Y. Ren, Y.C. Chou, P.K. Liaw, Adv. Mater. 32 (2020) 2004029.
[11] N.L. Okamoto, K. Yuge, K. Tanaka, H. Inui, E.P. George, AIP Adv 6 (2016) 125008.
[12] C. Wang, T.H. Li, Y.C. Liao, C.L. Li, J.S.C. Jang, C.H. Hsueh, Mater. Sci. Eng. A 764 (2019) 138192.
[13] S.P. Wang, J. Xu, J. Mater. Sci. Technol. 35 (2019) 812–816.
[14] S.P. Wang, J. Xu, Intermetallics 95 (2018) 59–72.
[15] J. Wang, S. Wu, S. Fu, S. Liu, Z. Ren, M. Yan, S. Chen, S. Lan, H. Hahn, T. Feng, J. Mater. Sci. Technol. 77 (2021) 126–130.
[16] Z. Yang, S. Lu, Y. Tian, Z. Gu, H. Mao, J. Sun, L. Vitos, J. Mater. Sci. Technol. 80 (2021) 66–74.
[17] L.R. Owen, N.G. Jones, J. Mater. Res. 33 (2018) 2954–2969.
[18] L.R. Owen, H.J. Stone, H.Y. Playford, Acta Mater 170 (2019) 38–49.
[19] L.R. Owen, N.G. Jones, Scr. Mater. 187 (2020) 428–433.
[20] Y.Y. Tan, M.Y. Su, Z.C. Xie, Z.J. Chen, Y. Gong, L.R. Zheng, Z. Shi, G. Mo, Y. Li, L.W. Li, H.Y. Wang, L.H. Dai, Intermetallics 129 (2021) 107050.
[21] F. Zhang, Y. Tong, K. Jin, H. Bei, W.J. Weber, A. Huq, A. Lanzirotti, M. Newville, D.C. Pagan, J.Y.P. Ko, Y. Zhang, Mater. Res. Lett. 6 (2018) 450–455.
[22] B. Fu, W.Y. Yang, L.F. Li, Z.Y. Zhao, Trans. Mater. Heat Treat. 38 (2017) 63–69 in Chinese.
[23] Z. Fu, W. Chen, H. Wen, D. Zhang, Z. Chen, B. Zheng, Y. Zhou, E.J. Lavernia, Acta Mater. 107 (2016) 59–71.
[24] N. An, Y. Sun, Y. Wu, J. Tian, Z. Li, Q. Li, J. Chen, X. Hui, Mater. Sci. Eng. A 798 (2020) 140213.
[25] B. Gludovatz, A. Hohenwarter, D. Catoor, E.H. Chang, E.P. George, R.O. Ritchie, Science 345 (2014) 1153–1158.
[26] Q. Ding, X. Fu, D. Chen, H. Bei, B. Gludovatz, J. Li, Z. Zhang, E.P. George, Q. Yu, T. Zhu, R.O. Ritchie, Mater. Today 25 (2019) 21–27.
[27] A. Gali, E.P. George, Intermetallics 39 (2013) 74–78.
[28] Q. Lin, J. Liu, X. An, H. Wang, Y. Zhang, X. Liao, Mater. Res. Lett. 6 (2018) 236–243.
[29] S.J. Sun, Y.Z. Tian, H.R. Lin, H.J. Yang, X.G. Dong, Y.H. Wang, Z.F. Zhang, Mater. Sci. Eng. A 740–741 (2019) 336–341.
[30] Z. Pu, Z.C. Xie, R. Sarmah, Y. Chen, C. Lu, G. Ananthakrishna, L.H. Dai, Philos. Mag. 101 (2020) 154–178.
[31] M. Naeem, H. He, F. Zhang, H. Huang, S. Harjo, T. Kawasaki, B. Wang, S. Lan, Z. Wu, F. Wang, Y. Wu, Z. Lu, Z. Zhang, C.T. Liu, X.L. Wang, Sci. Adv. 6 (2020) eaax4002.
[32] S.J. Sun, Y.Z. Tian, H.R. Lin, H.J. Yang, X.G. Dong, Y.H. Wang, Z.F. Zhang, Mater. Sci. Eng. A 712 (2018) 603–607.
[33] M. Naeem, H. He, S. Harjo, T. Kawasaki, F. Zhang, B. Wang, S. Lan, Z. Wu, Y. Wu, Z. Lu, C.T. Liu, X.-.L. Wang, Scr. Mater. 188 (2020) 21–25.
[34] F. Otto, Y. Yang, H. Bei, E.P. George, Acta Mater 61 (2013) 2628–2638.
[35] J. Ding, Q. Yu, M. Asta, R.O. Ritchie, Proc. Natl. Acad. Sci. USA 115 (2018) 8919–8924.
[36] S. Huang, W. Li, S. Lu, F. Tian, J. Shen, E. Holmström, L. Vitos, Scr. Mater. 108 (2015) 44–47.
[37] X. Sun, S. Lu, R. Xie, X. An, W. Li, T. Zhang, C. Liang, X. Ding, Y. Wang, H. Zhang, L. Vitos, Mater. Des. 199 (2021) 109396.
[38] S. Zhao, G.M. Stocks, Y. Zhang, Acta Mater. 134 (2017) 334–345.
[39] H. Van Swygenhoven, P.M. Derlet, A.G. Frøseth, Nat. Mater. 3 (2004) 399–403.
[40] Z. Lyu, X. Fan, C. Lee, S.Y. Wang, R. Feng, P.K. Liaw, J. Mater. Res. 33 (2018) 2998–3010.
[41] P. Koželj, S. Vrtnik, M. Krnel, A. Jelen, D. Gačnik, M. Wencka, Z. Jagličić, A. Meden, F. Danoix, J. Ledieu, M. Feuerbacher, J. Dolinšek, J. Magn. Magn. Mater. 523 (2021) 167579.
[42] K. Jin, B.C. Sales, G.M. Stocks, G.D. Samolyuk, M. Daene, W.J. Weber, Y. Zhang, H. Bei, Sci. Rep. 6 (2016) 20159.
[43] O. Schneeweiss, M. Friák, M. Dudová, D. Holec, M. Šob, D. Kriegner, V. Holý, P. Beran, E.P. George, J. Neugebauer, A. Dlouhý, Phys. Rev. B 96 (2017) 014437.
[44] D. Ma, B. Grabowski, F. Körmann, J. Neugebauer, D. Raabe, Acta Mater. 100 (2015) 90–97.
[45] Z. Dong, S. Schönecker, W. Li, D. Chen, L. Vitos, Sci. Rep. 8 (2018) 12211.
[46] S.M. Na, J.H. Yoo, P.K. Lambert, N.J. Jones, AIP Adv 8 (2018) 056412.
[47] Z. Dong, L. Vitos, Scr. Mater. 171 (2019) 78–82.
[48] D. Ma, M. Yao, K.G. Pradeep, C.C. Tasan, H. Springer, D. Raabe, Acta Mater 98 (2015) 288–296.
[49] S. Guo, C. Ng, Z. Wang, C.T. Liu, J. Alloys Compd. 583 (2014) 410–413.
[50] T. Degen, M. Sadki, E. Bron, U. König, G. Nénert, Powder Diffr 29 (2014) S13–S18.
[51] D. Molnár, X. Sun, S. Lu, W. Li, G. Engberg, L. Vitos, Mater. Sci. Eng. A 759 (2019) 490–497.
[52] G. Laplanche, M. Schneider, F. Scholz, J. Frenzel, G. Eggeler, J. Schreuer, Scr. Mater. 177 (2020) 44–48.
[53] G. Laplanche, P. Gadaud, O. Horst, F. Otto, G. Eggeler, E.P. George, J. Alloys Compd. 623 (2015) 348–353.
[54] A.J. Zaddach, C. Niu, C.C. Koch, D.L. Irving, Jom 65 (2013) 1780–1789.
[55] R. Naorem, A. Gupta, S. Mantri, G. Sethi, K.V. ManiKrishna, R. Pala, K. Balani, A. Subramaniam, Int. J. Mater. Res. 110 (2019) 393–405.
[56] M. Calamiotou, D. Lampakis, N.D. Zhigadlo, S. Katrych, J. Karpinski, A. Fitch, P. Tsiaklagkanos, E. Liarokapis, Phys. C-Supercond. Its Appl. 527 (2016) 55–62.
[57] L.R. Owen, E.J. Pickering, H.Y. Playford, H.J. Stone, M.G. Tucker, N.G. Jones, Acta Mater. 122 (2017) 11–18.
[58] W. Feng, Y. Qi, S. Wang, Mater. Res. Express 5 (2018) 106511.
[59] S. Huang, W. Li, X. Li, S. Schönecker, L. Bergqvist, E. Holmström, L.K. Varga, L. Vitos, Mater. Des. 103 (2016) 71–74.
[60] S. Huang, E. Holmström, O. Eriksson, L. Vitos, Intermetallics 95 (2018) 80–84.
[61] B. Zhang, Y. Duan, H. Zhang, S. Huang, G. Ma, T. Wang, X. Dong, N. Jia, J. Mater. Sci. Technol. 68 (2021) 124–131.
[62] Z. Dong, S. Huang, V. Ström, G. Chai, L.K. Varga, O. Eriksson, L. Vitos, J. Mater. Sci. Technol. 79 (2021) 15–20.
[63] P. Wei, Y. Fan, W. Zhang, X. Li, S. Zhu, J. Wang, C. Wang, T. Zhang, C. Chen, S. Guan, J. Magn. Magn. Mater. 519 (2021) 167432.
[64] R. Zhang, S. Zhao, J. Ding, Y. Chong, T. Jia, C. Ophus, M. Asta, R.O. Ritchie, A.M. Minor, Nature 581 (2020) 283–287.
[65] S. Qiu, X.C. Zhang, J. Zhou, S. Cao, H. Yu, Q.M. Hu, Z. Sun, J. Alloys Compd. 846 (2020) 156321.
[66] G. Laplanche, A. Kostka, C. Reinhart, J. Hunfeld, G. Eggeler, E.P. George, Acta Mater. 128 (2017) 292–303.
[67] Z. Wu, F. Tian, Mater. Today Commun. 25 (2020) 101336.
[68] J. Liu, X. Guo, Q. Lin, Z. He, X. An, L. Li, P.K. Liaw, X. Liao, L. Yu, J. Lin, L. Xie, J. Ren, Y. Zhang, Sci. China Mater. 62 (2019) 853–863.